Noncooperative Folding of Subdomains in Adenylate Kinase[†]

Louise Rundqvist, Jörgen Ådén, Tobias Sparrman, Marcus Wallgren, Ulrika Olsson, and Magnus Wolf-Watz*

Department of Chemistry, Umeå University, SE-901 87 Umeå, Sweden

Received September 22, 2008; Revised Manuscript Received December 20, 2008

ABSTRACT: Conformational change is regulating the biological activity of a large number of proteins and enzymes. Efforts in structural biology have provided molecular descriptions of the interactions that stabilize the stable ground states on the reaction trajectories during conformational change. Less is known about equilibrium thermodynamic stabilities of the polypeptide segments that participate in structural changes and whether the stabilities are relevant for the reaction pathway. Adenylate kinase (Adk) is composed of three subdomains: CORE, ATPlid, and AMPbd. ATPlid and AMPbd are flexible nucleotide binding subdomains where large-scale conformational changes are directly coupled to catalytic activity. In this report, the equilibrium thermodynamic stabilities of Adk from both mesophilic and hyperthermophilic bacteria were investigated using solution state NMR spectroscopy together with protein engineering experiments. Equilibrium hydrogen to deuterium exchange experiments indicate that the flexible subdomains are of significantly lower thermodynamic stability compared to the CORE subdomain. Using site-directed mutagenesis, parts of ATPlid and AMPbd could be selectively unfolded as a result of perturbation of hydrophobic clusters located in these respective subdomains. Analysis of the perturbed Adk variants using NMR spin relaxation and C^{α} chemical shifts shows that the CORE subdomain can fold independently of ATPlid and AMPbd; consequently, folding of the two flexible subdomains occurs independently of each other. Based on the experimental results it is apparent that the flexible subdomains fold into their native structure in a noncooperative manner with respect to the CORE subdomain. These results are discussed in light of the catalytically relevant conformational change of ATPlid and AMPbd.

Enzymes are remarkable biocatalysts that can accelerate chemical reactions with extraordinary specificity and efficacy. A fundamental principle in enzymology is that enzymes must be flexible in order to accommodate ligands, undergo conformational changes, and transfer functional groups. Flexibility can occur on various time scales, but motion in the microsecond to millisecond regime is often found to be relevant to enzymatic catalysis (*1*). A number of recent studies have shown that enzymes can show motion in substrate-free states similar to that during catalysis (*2*−*5*). Comprehension of how enzymes can lower transition state energies requires detailed knowledge of protein flexibility, which in turn depends on experimental quantification of flexibility and theoretical modeling of the basic physics of collective motion. Even though the importance of flexibility for enzymatic catalysis is appreciated, little is known about whether flexible segments in enzymes fold in a cooperative manner with respect to the global folding trajectory.

Scheme 1

$$AMP + ATP \underset{Mg^{2+}}{\overset{Mg^{2+}}{\rightleftarrows}} 2\,ADP$$

Adenylate kinase (Adk)[1] is a member of the NMP kinase family and catalyzes the magnesium-dependent reversible conversion of one AMP molecule and one ATP molecule into two ADP molecules (Scheme 1). Kinetic studies indicate that catalysis follows a random Bi−Bi mechanism for Adk (*6*).

Adk consists of three subdomains: the CORE subdomain and the ATP and AMP binding subdomains (ATPlid and AMPbd, respectively). Both ATPlid and AMPbd undergo large conformational changes in response to substrate binding and can interconvert between open and closed conformations (*7, 8*) (Figure 1). Similar interconversion between open and closed states is conserved within the NMP kinase family (*9*). The spatial translations in Adk occur on the microsecond to millisecond time scale and are rate-limiting for catalysis (*10*); thus, Adk is an enzyme where conformational flexibility is intimately linked to catalytic activity. Furthermore, the conformational change required for catalysis occurs already in the substrate-free

[†] Financial support for this work was provided by the Swedish Research Council (Grant 621-2004-923) and the Kempe Foundation to M.W.-W.

* To whom correspondence should be addressed. E-mail: magnus.wolf-watz@chem.umu.se. Tel: +46-90-786 76 90. Fax: +46-90-786 76 55.

[1] Abbreviations: Adk, adenylate kinase; AMPbd, AMP binding subdomain of Adk; Ap_5A, P^1,P^5-di(adenosine-5′-)pentaphosphate; ATPlid, ATP binding subdomain of Adk; CD, circular dichroism; CORE, core subdomain of Adk; CSI, chemical shift index; ΔG_{HX}, residue-specific thermodynamic stability; $\Delta G°_{NU}$, global thermodynamic stability in the direction of unfolding; k_{ex}, observed hydrogen exchange rate constant; k_{rc}, intrinsic hydrogen to deuterium exchange rate constant; mesoAdk, Adk isolated from *Escherichia coli*; m_{HX}, residue-specific denaturant dependency of ΔG_{HX}; m_{NU}, denaturant dependency of $\Delta G°_{NU}$; thermoAdk, Adk isolated from *Aquifex aeolicus*; HSQC, heteronuclear single-quantum coherence; NMP, nucleoside monophosphate; NMR, nuclear magnetic resonance; pD^{corr}, pD^{read} value corrected for the deuterium isotope effect; pD^{read}, pD value measured with a glass electrode; SOFAST-HMQC, band-selective optimized flip-angle short transient heteronuclear multiple-quantum coherence.

10.1021/bi8018042 CCC: $40.75
Published on Web 02/16/2009

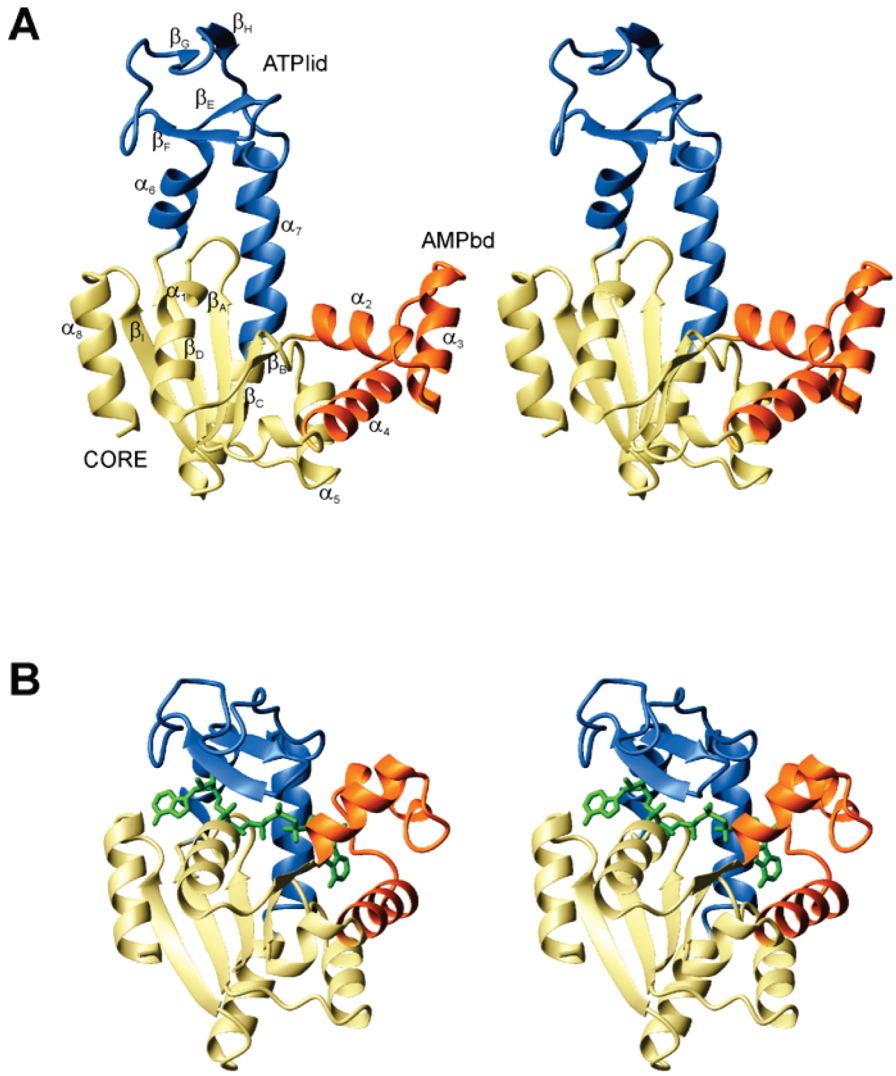

FIGURE 1: Crystallographic structures of mesoAdk in open and closed conformations. (A) Stereoview of the substrate-free open conformation (4AKE.pdb) of mesoAdk (*7*). (B) Stereoview of the closed conformation (1AKE.pdb) of mesoAdk in the presence of the tight binding inhibitor Ap_5A (green) (*8*). The subdomain arrangement is color-coded as follows: CORE (khaki), ATPlid defined as residues 113−176 (blue), and AMPbd defined as residues 31−72 (orange). Numbering of regular α-helices and *β*-strands is indicated. All illustrations of proteins in this paper were prepared using MolMol (*51*).

state (*5*). Addition of substrate acts to shift this sampling of conformational space toward the closed and active conformation (*11*). Recent experimental and computational findings indicate that Adk is an allosteric enzyme and that fluctuations in the ATPlid subdomain influence the dynamics in AMPbd (*11, 12*).

In this study, an NMR and protein engineering approach was used to address the cooperativity of subdomain folding in Adk. The approach was to characterize the equilibrium free energy of unfolding of Adk isolated from the mesophilic bacterium *Escherichia coli* (mesoAdk) and the hyperthermophilic bacterium *Aquifex aeolicus* (thermoAdk). By using solution state NMR spectroscopy, and in particular hydrogen to deuterium exchange experiments, C^{α} chemical shifts, and NMR spin relaxation lifetimes, a detailed structural map of local thermodynamic stabilities for both enzymes could be created. On the basis of the experimental results provided, it is shown that the flexible subdomains fold in a noncooperative manner with respect to the CORE subdomain. This feature is discussed in terms of the reaction pathway from the open to the closed state.

METHODS

Protein Preparation and Resonance Assignments. Both Adk variants were prepared as described previously (*10*). The NMR samples contained 1.0 mM ^{15}N-labeled or ^{15}N,^{13}C-labeled protein with 2 mM TCEP (only for experiments on mesoAdk), 50 mM NaCl, and 30 mM MES at pH 6.0 with 10% (v/v) $^{2}H_2O$ (NMR buffer). Triple resonance and hydrogen exchange NMR experiments were carried out on a Bruker DRX 600 MHz spectrometer equipped with a 5 mm triple resonance *z*-gradient cryoprobe. Three-dimensional ^{15}N NOESY-HSQC, HNHA (*13*), and ^{15}N T_2 relaxation (*14*) experiments were carried out on a Bruker DRX 500 MHz spectrometer. ^{15}N T_2 relaxation data were measured in an interleaved manner. NMR data were processed and visualized using the NMRPipe software (*15*) and ANSIG for Windows (*16*). Backbone resonance assignments of substrate-free mesoAdk and thermoAdk as well as ADP- and Ap_5A-saturated mesoAdk have been carried out previously (*10, 11*). ThermoAdk in the Ap_5A-bound state was assigned using ^{15}N NOESY-HSQC and HNHA experiments. Backbone reso-

Table 1: Relative Integrals of ^{31}P NMR Peaks in Figure 2

peak[a]	1	2	3	4
assignment	P^{α} (AMP)	P^{β} (ADP)	P^{β} (ATP)	P^{γ} (ATP)
relative integral[b]	1.00[c]	1.66 ± 0.01	0.99 ± 0.01	1.00 ± 0.01

[a] Peak numbering refers to the numbering in Figure 2. [b] Integrals are normalized to the intensity of the AMP P^{α} peak. [c] There is no error indicated for the AMP peak since this peak is used for normalization.

nance assignments for the ATPlid and AMPbd mutants were obtained using combinations of ^{15}N NOESY-HSQC, HNHA (*13*), HNCA (*17*), HNCACB (*18*), CBCA(CO)NH (*19*), and CC(CO)NH (*20*) experiments. ThermoAdk in the pH range 6.0−9.9 was assigned by following the pH dependency of resonances in SOFAST-HMQC spectra (*21*). One-dimensional ^{31}P NMR experiments were carried out on a Bruker DRX 500 MHz spectrometer using a recycling delay of 10 s. Integration of peaks was performed using Lorentzian deconvolution functions in Topspin 2.0. Peak intensities were estimated by averaging of peak integrals in three independent spectra after equilibration of 1 mg of mesoAdk with 20 mM ADP (Table 1). The α-phosphates of ADP and ATP were not included when calculating the equilibrium constant due to spectral overlap. Assignment of peaks was performed by collecting reference spectra of AMP, ADP, and ATP in the absence of Adk. All NMR experiments were performed at 19.7 °C, and the temperature was calibrated by inserting a thermoelement into the probe.

Hydrogen Exchange. To account for the kinetic isotope effect, the observed pD values (pD^{read}) were corrected with a factor of 0.4 ($pD^{corr} = pD^{read} + 0.4$) (*22*). For measurements of hydrogen exchange, protonated protein samples were lyophilized overnight. Addition of ^2H_2O to the appropriate volume was performed at 4 °C, with subsequent adjustment of pD^{read} to 6.0−6.2. Samples were transferred to an NMR tube, inserted into the magnet, and equilibrated to a sample temperature of 19.7 °C. Exchange kinetics was followed by collecting ^{1}H−^{15}N HSQC spectra over 2−3 days. For measurement of hydrogen exchange as function of pD for thermoAdk, a concentrated solution of thermoAdk in 25 μL of NMR buffer was diluted in 375 μL of ^2H_2O directly in the NMR tube. This procedure resulted in a dead time of 80 s before the first SOFAST-HMQC experiment was started. The experiments were performed with a relaxation delay of 100 ms, 512 data points in the directly detected dimension, and 100 data points in the indirectly detected dimension, resulting in an experimental time of 51 s.

Mutagenesis. Artificial sequences for the ATPlid and AMPbd mutants were ordered from GENEART (Germany). The sequences encoding the mutant proteins were subcloned into the expression vector pET-3a (Novagen) using the restriction enzymes *Nde*1 and *Bam*HI. The final constructs were verified using DNA sequencing (Eurofins MWG Operon, Germany). Protein purification was performed in the same manner as for mesoAdk.

Data Analysis. To separate the contribution of local fluctuations to calculated ΔG_{HX} values, the denaturant dependency of ΔG_{HX} was treated as described in refs *23* and *24*:

$$\Delta G_{HX} = -RT \ln(K_{unf} + K_{fl}) \quad (1)$$

$$K_{unf} = e^{(-\Delta G_{unf} + m_{HX}[D])/RT} \quad (2)$$

$$K_{fl} = e^{-\Delta G_{fl}/RT} \quad (3)$$

Here, K_{unf} and K_{fl} represent the equilibrium constants for cooperative and local unfolding and ΔG_{unf} is the residue-specific thermodynamic stability extrapolated to native conditions. The denaturant dependency of ΔG_{unf} is given by m_{HX} and the denaturant concentration by [D].

The midpoint of each ^{1}H−^{15}N HSQC experiment was used to construct the time vector used to fit k_{ex} rates. T_2 relaxation lifetimes, k_{ex} rates, and ΔG_{HX} values were quantified using in-house written Matlab routines, based on the Levenberg−Marquart method (*25*), which are available upon request. Integration of peaks was performed using routines in NMRpipe. Standard errors in k_{ex} and T_2 were estimated from the noise level of the data combined with the curvature around the χ^2 minima. The estimated error in ΔG_{HX} contains contributions from the fitted k_{ex} and from the calculated k_{rc}, through its pD dependence. The uncertainty of the pD measurement was estimated to be ±0.05 pD units. The specified ΔG_{HX} errors are slightly asymmetric, since the error propagation was calculated by direct insertion of the limiting rates in the nonlinear eq 6 and by assuming independent errors in k_{ex} and k_{rc}. For residues that have very slow k_{ex} rates ($<10^{-5}$ min^{-1}), corresponding to less than 3% decay in 2 days, the error interval is deliberately set extremely wide to illustrate that only the lower limit of ΔG_{HX} can be estimated.

RESULTS

Equilibrium Constant of Scheme 1. Adk has residual activity even without addition of Mg^{2+}, which was the experimental condition used in this study. Addition of ADP to mesoAdk generates an equilibrium mixture of AMP, ATP, and ADP according to Scheme 1. The equilibrium constant in the direction of ADP formation in the absence of added Mg^{2+} was estimated to be 2.8 ± 0.1 at 19.7 °C based on ^{31}P NMR peak intensities (Figure 2 and Table 1). As a consequence, addition of millimolar amounts of ADP will generate millimolar concentrations of all three relevant nucleotides.

Local Stabilities Derived from Hydrogen Exchange. To investigate the structural distribution of free energies of unfolding in Adk, mesoAdk and thermoAdk were analyzed using solution state NMR spectroscopy. NMR-based hydrogen exchange experiments can provide equilibrium thermodynamics of protein folding and local fluctuations to the level of individual amino acid residues. Measurement of exchange kinetics in the EX2 regime yields residue-specific equilibrium constants for disruption of hydrogen bonds, from which thermodynamic stabilities (ΔG_{HX}) of hydrogen-bonded amide protons can be calculated (*26*). Hydrogen to deuterium exchange kinetics is sensitive to the protein folding trajectory and can be used to deconvolute complex reactions that deviate from an idealized two-state folding model (*23, 24, 27, 28*). For a two-state folding model where the disruption of hydrogen bonds is dictated by global unfolding of the protein, ΔG_{HX} should in principle converge around the global stability measured by independent methods. However, *cis*−*trans* isomerization of proline residues is not detected in hydrogen exchange experiments and may cause a significant deviation of the thermodynamic stability measured with global methods even for a two-state model (*29*).

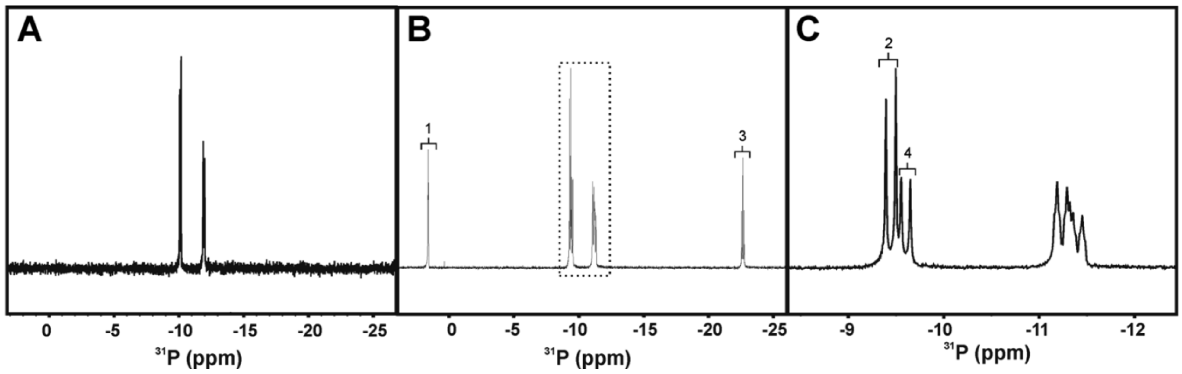

FIGURE 2: ^{31}P NMR spectra of ADP in the absence and presence of mesoAdk. (A) One-dimensional ^{31}P reference spectrum of 20 mM ADP. (B) One-dimensional ^{31}P spectrum of 20 mM ADP equilibrated with 1 mg of mesoAdk. (C) Expansion of the dotted part of panel B. Assignment of peaks relevant for determination of the equilibrium constant in the direction of ADP formation is indicated with numbers: 1, P^{α} of AMP; 2, P^{β} of ADP; 3, P^{β} of ATP; 4, P^{γ} of ATP. The relative concentrations of components were determined by integration of the phosphate peaks. Integration of the overlapping peaks was performed using Lorentzian deconvolution. The experiment in panel B was repeated three times to estimate the standard deviation of the equilibrium constant. Mean relative peak integral values that was used for calculation of the equilibrium constant are shown in Table 1.

ΔG_{HX} can also be influenced by local fluctuations, which may be described as "breathing" of secondary structure elements (*26*), allowing ^2H_2O to exchange with amide protons. Local fluctuations can therefore obscure the protein folding/unfolding contribution to ΔG_{HX}. In order to use hydrogen exchange for understanding the equilibrium thermodynamics of a protein folding reaction, it is important to (i) deconvolute the contribution to ΔG_{HX} from local fluctuations and (ii) apply an appropriate folding model. If structural elements show ΔG_{HX} values that deviate significantly from the global stability but cannot be explained by local fluctuations or proline *cis*−*trans* isomerization, a more complex folding model than global two state can be justified.

The observed hydrogen exchange rates (k_{ex}) of backbone amide protons were determined by fitting the time dependence of integrated signal intensities in $^1H-^{15}N$ HSQC NMR spectra to single exponential decays. Hydrogen exchange was analyzed using the Linderstrøm−Lang scheme (*30*):

$$NH_{closed} \underset{k_{cl}}{\overset{k_{op}}{\rightleftharpoons}} NH_{open} \xrightarrow{k_{rc}} ND \quad (4)$$

Here, k_{cl} and k_{op} are rate constants for formation and disruption of protecting hydrogen bonds and k_{rc} is the intrinsic residue-specific exchange rate calculated as described earlier (*31*). In the limit of EX2 exchange (*30*), i.e., $k_{cl} \gg k_{rc}$, k_{ex} equals

$$k_{ex} = \frac{k_{op}k_{rc}}{k_{cl}} = K_{op}k_{rc} \quad (5)$$

where K_{op} is the equilibrium constant for disruption of hydrogen bonds. Local stabilities (ΔG_{HX}) are then calculated according to the relation formulated by Englander and coworkers (*26*):

$$\Delta G_{HX} = -RT \ln K_{op} = -RT \ln\left(\frac{k_{ex}}{k_{rc}}\right) \quad (6)$$

pD Dependency of Hydrogen Exchange Rates. The hydrogen exchange experiments used for quantitative analysis in this study were performed at a pD^{read} close to 6.0. Since eq 5 is valid only in the EX2 regime, verification of these conditions at pD^{read} around 6.0 is important. In the EX2 regime a plot of $\log(k_{ex})$ vs pD should result in a straight line with a slope of unity under the assumption that the protein stability is pD independent. EX2 conditions were verified for thermoAdk by analysis of k_{ex} as a function of pD^{read} in the interval 6.2−9.9 (Figure 3A). Most of the observable residues remain in the EX2 regime over the entire pD interval, enabling the use of eq 6 for determination of ΔG_{HX}. However, some residues in ATPlid show a slope that is smaller than 1, indicating that the exchange is not strictly EX2. To verify EX2 conditions for mesoAdk, hydrogen exchange rates were compared at a pD^{read} of 6.0 and 7.2 (Figure 3B). EX2 conditions are valid for the majority of residues in mesoAdk, but as for thermoAdk, some residues in the ATPlid subdomain deviate from EX2 behavior. Residues that deviated from ideal EX2 behavior were still analyzed using the formalism developed from EX2 exchange since deviation from EX2 can lead to overestimation and not underestimation of quantified ΔG_{HX} values. For both mesoAdk and thermoAdk, quantified ΔG_{HX} in ATPlid values are consistently lower than those of CORE residues as shown in the following sections; thus a minor deviation from EX2 does not qualitatively change the interpretation of obtained results.

Structural Distribution of ΔG_{HX} in ThermoAdk. In Figure 4A, ΔG_{HX} values quantified using hydrogen exchange experiments for substrate-free thermoAdk are displayed on the crystallographic substrate-free structure. Residues with similar ΔG_{HX} fall into distinct clusters with the most stable substructure located in the CORE subdomain. Several residues in both thermoAdk and mesoAdk display k_{ex} rates that are too slow to enable quantification; these residues are assigned a lower limit of ΔG_{HX} equal to 29 kJ mol^{-1}. Residues in the ATPlid and AMPbd subdomains of thermoAdk display lower ΔG_{HX} values compared to CORE residues, indicating that the individual subdomains of thermoAdk do not fold with one cooperative transition. Some residues, primarily in ATPlid and AMPbd, have exchanged completely within the dead time of the experiment. A plot of the ΔG_{HX} values as function of primary sequence is shown in Figure 4B. In order to overcome the limitation of missing data in the flexible subdomains, we made use of the fact that binding of a ligand to a protein will increase the apparent stability of the protein by shifting the native ensemble further

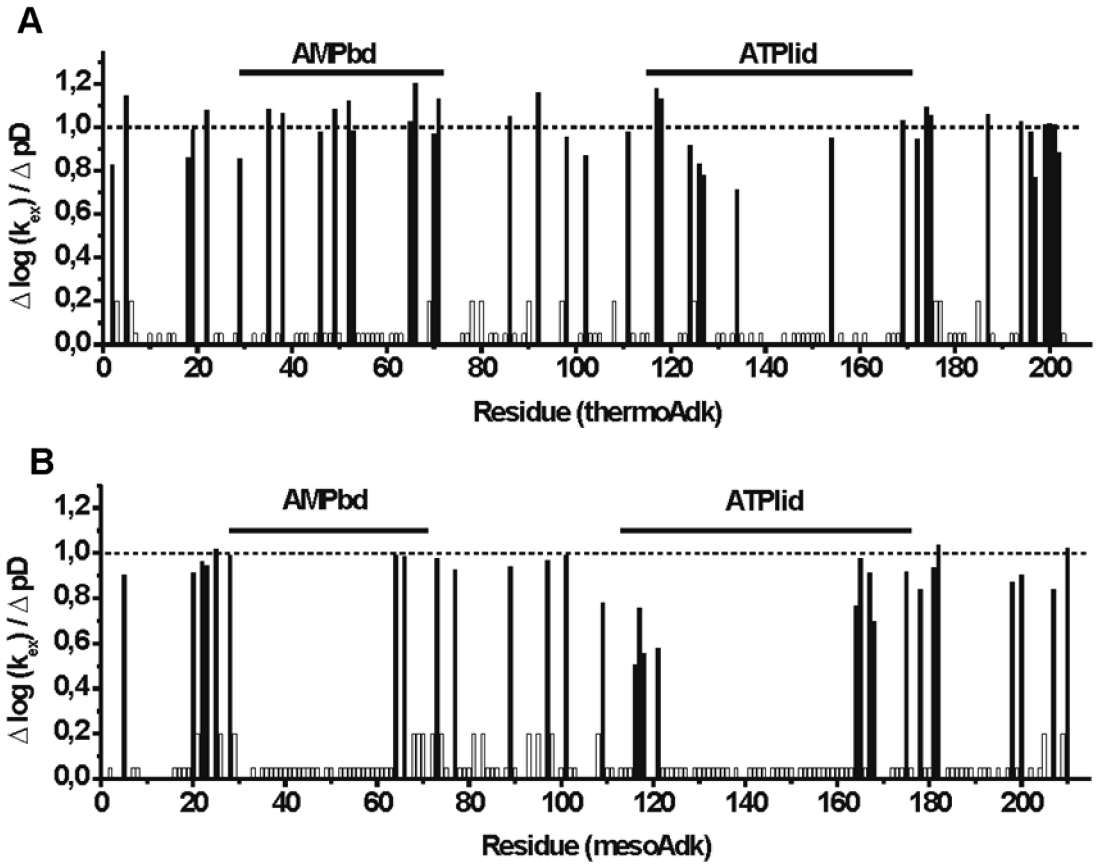

FIGURE 3: pD dependencies of hydrogen exchange rates in meso- and thermoAdk. The pD dependency of hydrogen exchange rates, $\Delta\log(k_{ex})/\Delta$pD, is plotted against the primary sequence (black bars). Unassigned, overlapped, or proline residues are not shown. Residues that could not be analyzed due to either too rapid or too slow exchange are given artificial values of 0.05 and 0.2, respectively (white bars). The location of AMPbd (residues 31−72 in mesoAdk and thermoAdk) and ATPlid (residues 113−176 in mesoAdk and 114−170 in thermoAdk) is indicated with solid lines. Ideal EX2 behavior is indicated with a dotted line. (A) Results for thermoAdk analyzed by comparing k_{ex} rates in the pD^{read} interval 6.2−9.9. (B) Results for mesoAdk evaluated at pD^{read} 6.0 and 7.2.

away from the unfolded state in the free energy landscape (*32*). The apparent folding equilibrium constant for a protein stabilized by a ligand bound in a 1:1 ratio is given by

$$K^{app} = \frac{[N] + [NL]}{[U]} \quad (7)$$

where [N] is the concentration of folded enzyme, [NL] is the concentration of ligand-bound enzyme, and [U] is the concentration of unfolded enzyme. The apparent stability of thermoAdk was increased by adding the tight binding substrate-mimicking inhibitor Ap_5A. From a structural perspective, the use of the inhibitor Ap_5A is reasonable, since the solution structures of mesoAdk in complex with the natural substrate ADP or the inhibitor Ap_5A are virtually identical (*11*). The dissociation constant for binding of Ap_5A to mesoAdk is 2.5 nM (*33*). Binding of Ap_5A to thermoAdk is slow on the NMR time scale (data not shown), which indicates strong binding also to thermoAdk. Due to the strong binding, Adk can readily be saturated by adding stochiometric concentrations of Ap_5A. Measurement of hydrogen exchange for thermoAdk with a 2-fold molar excess of Ap_5A enabled quantification of many amide protons that exchanged within the experimental dead time in the substrate-free state (Figure 4C,D). The pattern with ATPlid and AMPbd being less stable than the CORE subdomain in thermoAdk is confirmed in the Ap_5A-stabilized hydrogen to deuterium exchange experiment. In summary, by quantifying ΔG_{HX} both for the ligand-free enzyme and in the presence of the inhibitor Ap5A, a detailed structural map of local thermodynamic stabilities on the folding free energy landscape for thermoAdk could be created.

Structural Distribution of ΔG_{HX} in MesoAdk. Compared to thermoAdk, the structural distribution of ΔG_{HX}, albeit with overall lower values, is conserved in mesoAdk in the substrate-free state. Most residues in ATPlid and AMPbd exchange completely within the dead time of the experiment (Figures 3B and 5A,B), indicating that their thermodynamic stabilities on average are significantly lower than those of CORE. As a consequence it appears that also mesoAdk folds with more than one cooperative transition. Stabilization of the enzyme by binding Ap_5A was employed also in mesoAdk to increase the number of observable residues in the flexible subdomains. Quantified ΔG_{HX} values in the Ap_5A-bound state show that ATPlid and AMPbd are thermodynamically less stable than the CORE subdomain also in the mesophilic enzyme (Figure 5C,D). In order to verify the relevance of experiments performed with Ap_5A, ΔG_{HX} values for mesoAdk were measured in the ADP-saturated state, i.e., AMP, ADP, and ATP present according to Scheme 1. The presence of three different nucleotides could complicate the interpretation of the experiment. However, it has been shown using residual dipolar couplings that the average solution structure of both the Ap_5A- and ADP-bound states primarily populates a conformation that strongly resembles the crystallographic closed state (*11*). During catalysis, both the open and closed

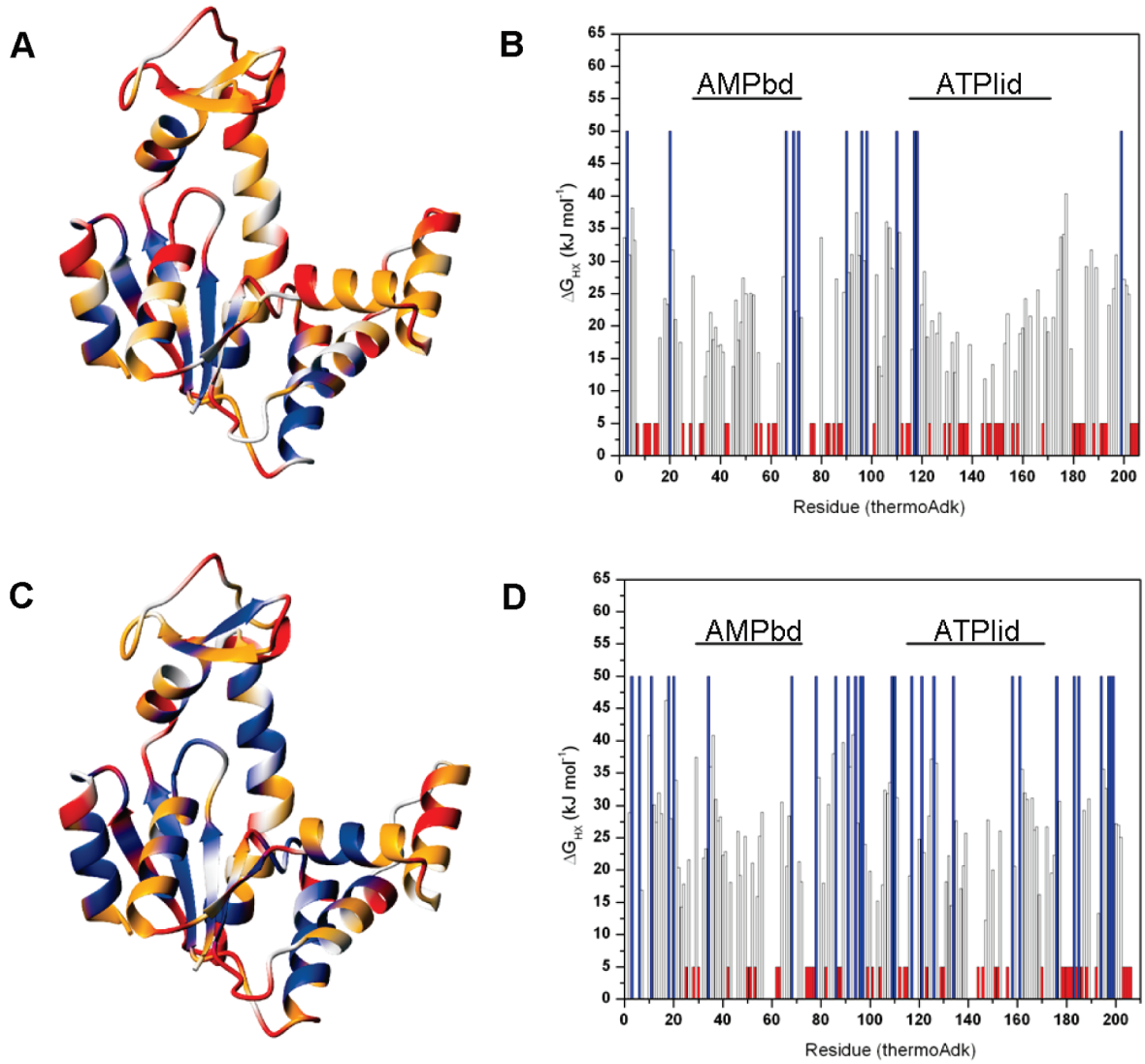

FIGURE 4: Local stabilities (ΔG_{HX}) of thermoAdk in substrate-free and Ap5A-bound states quantified by hydrogen to deuterium exchange. (A, B) Substrate-free thermoAdk. (C, D) Ap_5A-bound thermoAdk. In (A) and (C) the ΔG_{HX} values are plotted on the crystal structure of substrate-free open thermoAdk using molecule A in the asymmetric unit (*5*). ΔG_{HX} values are color-coded on the structure according to $\Delta G_{HX} > 29$ kJ mol^{-1} (blue) and $29 > \Delta G_{HX} > 11$ kJ mol^{-1} (orange), residues that exchange completely within the dead time of the experiment (red), and overlapping, unassigned, or proline residues (white). In (B) and (D) the fitted ΔG_{HX} values are plotted against primary sequence. Blue bars represent residues that exchange too slowly for quantification, and red bars represent residues that exchange within the deadtime of the experiment. For illustrative purposes the ΔG_{HX} values of these extreme cases are given values of 50 and 5 kJ mol^{-1}, respectively. ATPlid and AMPbd subdomains are indicated as solid lines. Fitted ΔG_{HX} values for thermoAdk are summarized in Supporting Information Table S1.

states can be detected using relaxation dispersion experiments; this conformational equilibrium is strongly skewed toward the closed conformation (*10*), in good agreement with measured residual dipolar couplings (*11*). The main contribution to ΔG_{HX} in both Ap_5A- and ADP-bound states consequently arises from the closed conformation. Saturation was accomplished by addition of 20 mM ADP to the enzyme (*11*). Analysis of hydrogen exchange for the mesoAdk−ADP complex (Figure 5E,F) resulted in a very similar spatial distribution of ΔG_{HX} values compared to the Ap_5A-bound state. As a consequence, it is shown that the stability of the flexible ATPlid and AMPbd subdomains are thermodynamically less stable than the CORE subdomain in mesoAdk. In principle, the low thermodynamic stability of ATPlid and AMPbd can reflect local fluctuations and not free energy differences between folded and unfolded states. In order to examine whether the free energy landscape of folding for mesoAdk is accurately defined using the hydrogen exchange experiments performed under native conditions, the contribution of local fluctuations to observed ΔG_{HX} values is addressed in the section below.

Identification of Foldons in MesoAdk. An emerging view is that some proteins are built of cooperatively folding units denoted as foldons (*28*) and formation of the native folded state can follow a trajectory where native-like foldons are assembled in an ordered way. Foldons can be identified by observing the denaturant dependence of ΔG_{HX} (*23*). The main driving force in denaturant-induced unfolding of proteins is the difference in solvent-accessible surface area between folded and unfolded states (*34*). Local fluctuations are not sensitive to denaturant because the difference in solvent-accessible surface area between the states involved in a local fluctuation is small. Hydrogen exchange measured at low denaturant concentrations can be used to determine the equilibrium constant of a local fluctuation (eqs 1−3). When the denaturant concentration is approaching the midpoint of

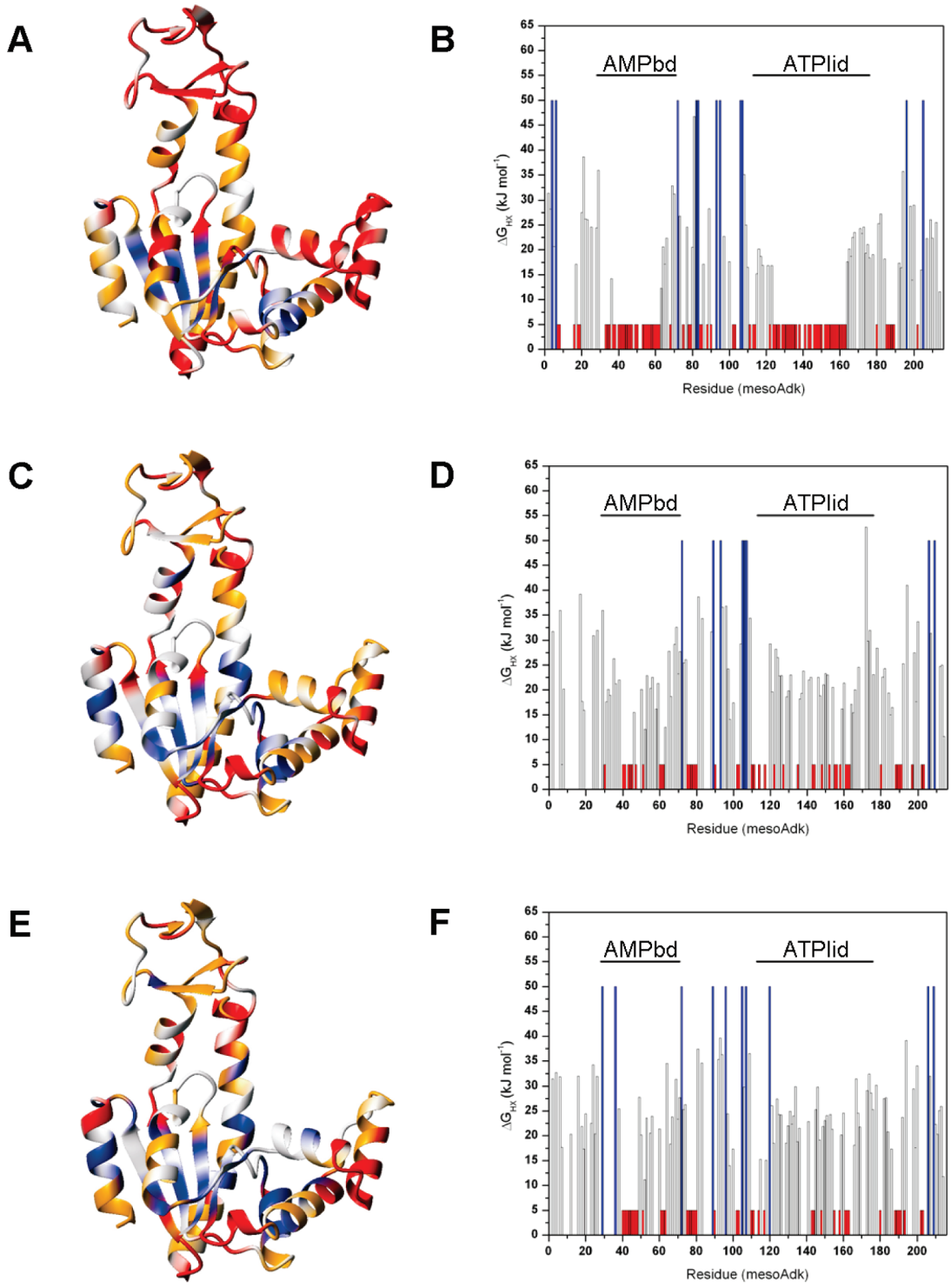

FIGURE 5: Local stabilities (ΔG_{HX}) of mesoAdk in free and bound states quantified by hydrogen to deuterium exchange. (A, B) Substrate-free mesoAdk. (C, D) Ap_5A-bound mesoAdk. (E, F) ADP-saturated mesoAdk. In (A), (C), and (E) results are displayed on the open mesoAdk structure (4AKE.pdb) with the same color coding as in Figure 4. (B), (D), and (F) show fitted values plotted against primary sequence (color coding as in Figure 4). ATPlid and AMPbd subdomains are indicated as solid lines. Fitted ΔG_{HX} values for mesoAdk are summarized in Supporting Information Table S2.

global unfolding, ΔG_{HX} will be dominated by unfolding of foldons, and the denaturant dependency of ΔG_{HX} in this regime can provide residue-specific m values (m_{HX}) and the residue-specific stability in water (ΔG_{unf}). Within foldons, the m_{HX} values should converge around one well-defined value (*23*). For mesoAdk the midpoint of urea-induced unfolding was determined to be 3.5 ± 0.6 M urea in ^2H_2O using CD spectroscopy (Figure 6). ThermoAdk is not suitable for these experiments since it cannot be denatured using urea and requires large concentrations of guanidine hydrochloride for global unfolding (midpoint of unfolding 4.4 M; data not shown). Under these high salt conditions, the NMR cryoprobe loses most of its additional sensitivity, making accurate quantification of k_{ex} rates unfeasible. Therefore, foldons were only quantified for mesoAdk. In order to identify foldons, the residue-specific thermodynamic stability as a function of urea concentration was fitted to eqs 1−3. The identification of foldons was performed based on similarity in m_{HX} values,

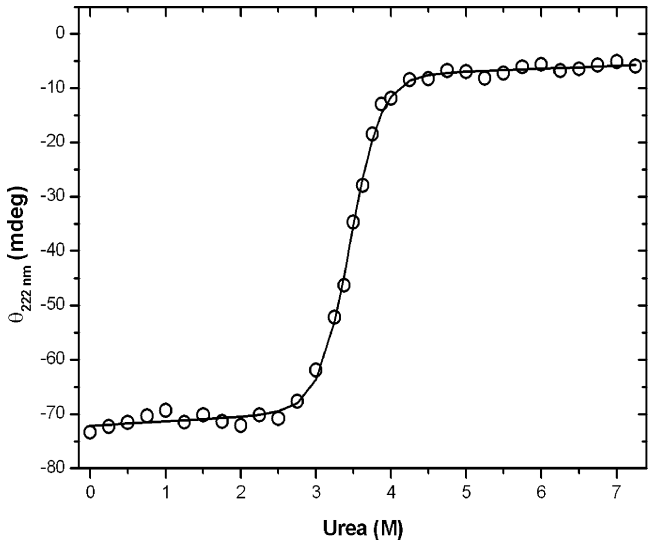

FIGURE 6: Global thermodynamic stability of mesoAdk in ^2H_2O. Urea-induced unfolding was followed by monitoring the CD signal at 222 nm. The experiment was performed in the NMR buffer using ^2H_2O as solvent, and the observed CD signal was fitted to a two-state model (*52*). The fitted parameters are $\Delta G^\circ_{NU} = 40.8 \pm 5.0$ kJ mol^{-1} and $m_{NU} = 11.8 \pm 1.4$ kJ mol^{-1} M^{-1}, where ΔG°_{NU} is the global stability extrapolated to native conditions and m_{NU} the denaturant dependency of ΔG°_{NU} in the direction of unfolding.

where a foldon is defined as a cluster of residues that have similar m_{HX} values and are located in close proximity to each other in the three-dimensional structure (*23, 24*). In Figure 7G, all fitted m_{HX} values are plotted against primary sequence and color-coded according to grouping of foldons. Based on quantifiable m_{HX} values, three distinct foldons with separable denaturant dependencies of ΔG_{HX} could be identified for mesoAdk, of which two belong to the CORE subdomain and one to ATPlid (Figure 7). In Figure 7, global unfolding parameters (ΔG°_{NU} and m_{NU}) of mesoAdk obtained using CD spectroscopy are represented as a dotted line for reference. All identified foldons group structurally with polypeptide segments that are stabilized with extensive intramolecular contacts. Foldon 1 is composed of residues that belong to the CORE subdomain, and it is characterized by an average m_{HX} value of 12.0 ± 1.7 kJ mol^{-1} M^{-1} that is in good agreement with the m_{NU} value (11.8 ± 1.4 kJ mol^{-1} M^{-1}) for global unfolding (Figures 6 and 7A,C). In addition to CORE residues identified by comparison of the crystal structures of mesoAdk in the open and closed states (Figure 1), the hydrogen exchange data suggest that residues 68−73 in helix α4, previously considered to be part of the AMPbd subdomain, thermodynamically belong to foldon 1. Since ΔG_{HX} values of residues in foldon 1 show clear curvature and m_{HX} values that coincide with the global m_{NU} value when analyzed as a function of urea, residues in foldon 1 exchange through global unfolding of the enzyme at urea concentrations above 2 M. However, under native conditions, local fluctuation is the dominating contribution to hydrogen exchange. Foldon 2 (Figure 7B,C) is composed of CORE residues 174−210, including the C-terminal residues of helix α_7, helix α_8, and strand β_I and is characterized by an average m_{HX} value of 7.8 ± 1.7 kJ mol^{-1} M^{-1}, which is significantly lower than the global m_{NU} value. Hydrogen exchange in foldon 2 under native conditions is also strongly influenced by local fluctuations, whereas exchange at high denaturant concentrations is dominated by subunit unfolding. Foldon 3 is composed of helix α_6 and helix α_7 in ATPlid that display an average m_{HX} value of 2.8 ± 0.9 kJ mol^{-1} M^{-1}, which is significantly lower than those quantified for the two CORE foldons (Figure 7D,F). Residues in foldon 3 show linear dependencies of ΔG_{HX} versus urea concentration; this behavior does not enable separation of the contributions from local fluctuations and subunit unfolding to ΔG_{HX}, and these residues were fitted according to eq 2. Since the quantifiable residues in ATPlid are displaying similar denaturant dependencies of ΔG_{HX} values, and local fluctuations are unaffected by denaturant (*35*), the hydrogen exchange data indicate that the ATPlid behaves as one cooperative unit with respect to folding. Because of the lack of curvature in the denaturant dependency in Figure 7D we cannot deconvolute the contribution from local fluctuations nor conclusively conclude that exchange occurs due to complete subunit unfolding of ATPlid. Based on this argument fitted ΔG_{unf} values in ATPlid may actually report on a state that differs from a completely unfolded ATPlid. The residues shown in Figure 7D do not coincide perfectly, which might depend on residue-specific contributions from local fluctuations. Most residues in the AMPbd are completely exchanged within the dead time of the experiment, except for residues 63−66 in helix α_4 and Arg36, which exchange mainly through local fluctuations. Given that the C-terminal part of AMPbd (residues 68−73) is reassigned to the CORE subdomain with respect to thermodynamic stability, no distinct foldon could be identified in AMPbd using these experiments. Finally, some residues primarily located in the CORE subdomain show no detectable denaturant dependency, which means that local fluctuations are dominating the exchange process (Figure 7E,F). From a mechanistic viewpoint it is not trivial to understand why residues within foldons can deviate with respect to denaturant dependency; one should however bear in mind that local fluctuation is a poorly understood phenomenon. In light of the absence of a convincing physical model that can explain these fluctuations we conclude that there exist residues in foldons 1 and 2 that may or may not be consistent with our mapping of foldons. The average thermodynamic stability of residues in foldons 1, 2, and 3 extrapolated to native conditions is 51 ± 4.0, 36 ± 5.8, and 20 ± 3.0 kJ mol^{-1}, respectively. The ΔG°_{NU} obtained from CD spectroscopy is 40.8 ± 5.0 kJ mol^{-1}. Clearly, the global stability obtained from CD spectroscopy is lower than what was estimated from the hydrogen exchange experiments. This observation has been made for several other proteins, and a large fraction of this discrepancy can be explained with proline *cis*−*trans* isomerization (*36*). The free energy contribution from proline *cis*−*trans* isomerization to ΔG_{HX} for Adk was calculated as outlined in ref *29* using tabulated values of the equilibrium constant for *cis*−*trans* isomerization (*37*). MesoAdk has 10 prolines, one of which is in the *cis* conformation (Pro87), which equals a free energy contribution of 5.7 kJ mol^{-1}. With this correction factor the ΔG°_{NU} values from CD and ΔG_{unf} from hydrogen exchange overlap within the error margins. There exists a correlation between the average ΔG_{unf} and ΔG_{HX} values obtained under native conditions in the absence of denaturants. Residues in CORE that have high stability extraploated to native conditions also have high ΔG_{HX} values. Conversely, quantifiable residues in ATPlid that display low ΔG_{unf} values also display low ΔG_{HX} values. This result highlights the fact that the

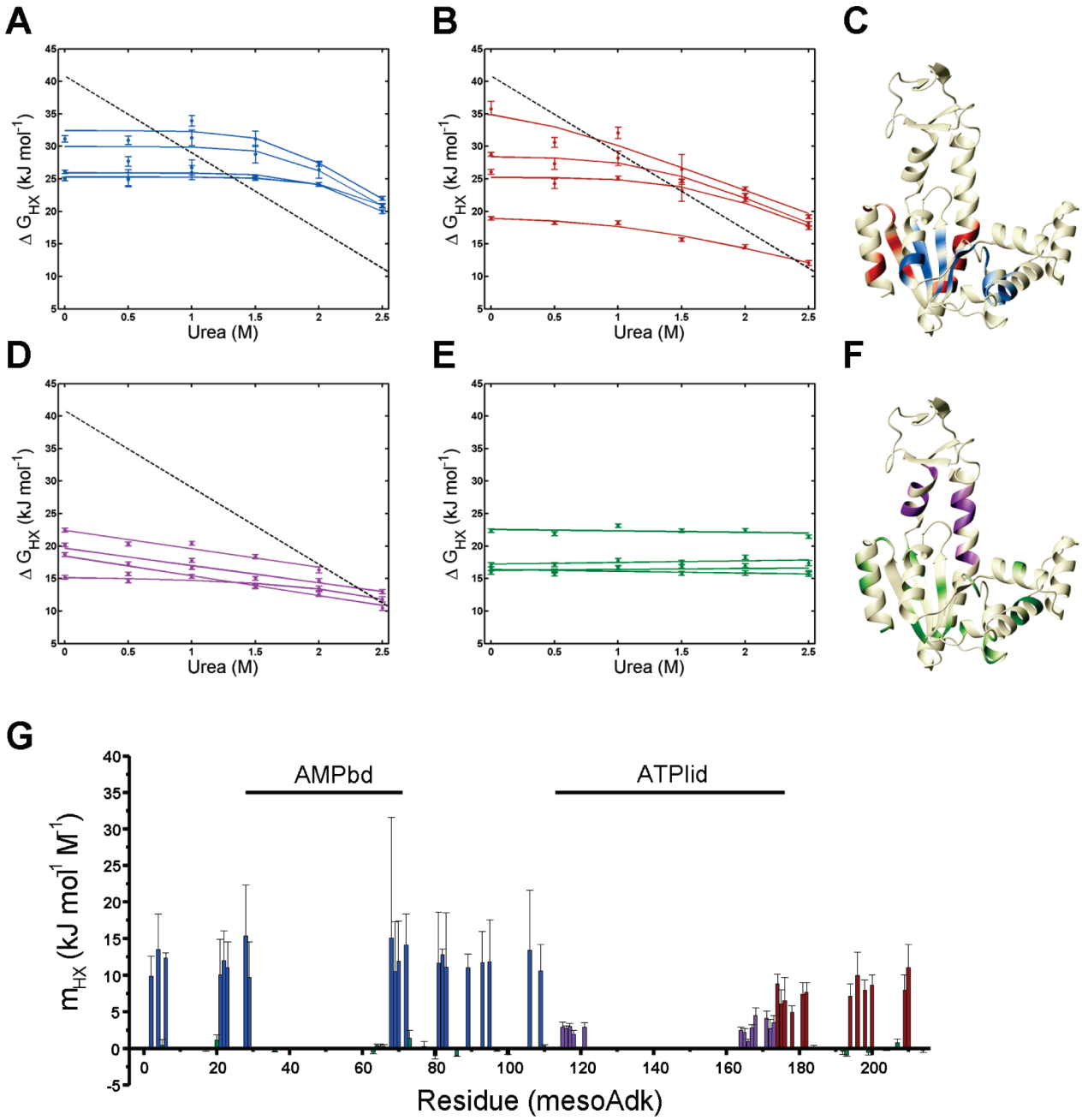

FIGURE 7: Foldon substructure in mesoAdk. ΔG_{HX} values were determined under mildly denaturing conditions, and the amino acid residues were clustered into four different groups according to their denaturant dependencies. ΔG_{HX} and experimental uncertainties for representative residues in each foldon are plotted as a function of urea concentration. Best fitted urea dependencies of ΔG_{HX} according to eqs 1−3 are shown as lines. In (A), (B), and (D) the dotted straight line corresponds to global stability and m_{NU} values obtained by CD spectroscopy. (A) Foldon 1 is characterized by m_{HX} values in good agreement with the global m_{NU} value and comprises residues in CORE and the C-terminal part of helix α4 in AMPbd. Shown are residues Lys23, Glu70, Ala93, and Phe109. (B) Foldon 2 is a substructure of CORE, consisting of the C-terminal part of helix α7, helix α8, and strand β_I, which is characterized by lower m_{HX} values compared to foldon 1. Foldon 2 is represented by residues Leu178, Ala194, Gly198, and Leu209. (C) Foldon 1 (blue) and foldon 2 (red) shown on the open mesoAdk structure. (D) Foldon 3 comprises residues in helices α6 and α7 in ATPlid and displays significantly lower m_{HX} values compared to foldons 1 and 2. Representative data for foldon 3 are shown with residues Leu115, Ile116, Val117, and Arg167. (E) Residues that show no observable denaturant dependencies of ΔG_{HX} are illustrated with residues Ala17, Ala66, Asp110, and Glu204. (F) Foldon 3 (purple) and residues in (E) (green) displayed on the open mesoAdk structure. (G) Plot of m_{HX} values against primary sequence. Residues are color-coded as follows: foldon 1 (blue), foldon 2 (red), foldon 3 (purple), and group 4 (green). All fitted parameters from the denaturant dependency of ΔG_{HX} values in mesoAdk are summarized in Supporting Information Table S3.

presence of local fluctuations does not qualitatively influence the structural map of local thermodynamic stabilities obtained for mesoAdk using ΔG_{HX} values (Figure 5). On the basis of this argument we suggest that ΔG_{HX} values can be used also for thermoAdk to create a relevant structural map of local free energies of folding. Nevertheless, it is apparent that virtually all residues in mesoAdk are influenced by local fluctuations under native solvent conditions; thus the structural map in Figure 5 may also be viewed as the strength of hydrogen bonds that are being broken during local fluctuations.

Protein Engineering. The large difference in ΔG_{HX} between the CORE and ATPlid and AMPbd for both mesoAdk and thermoAdk, together with the identification of the ATPlid as a foldon in mesoAdk, suggests that folding

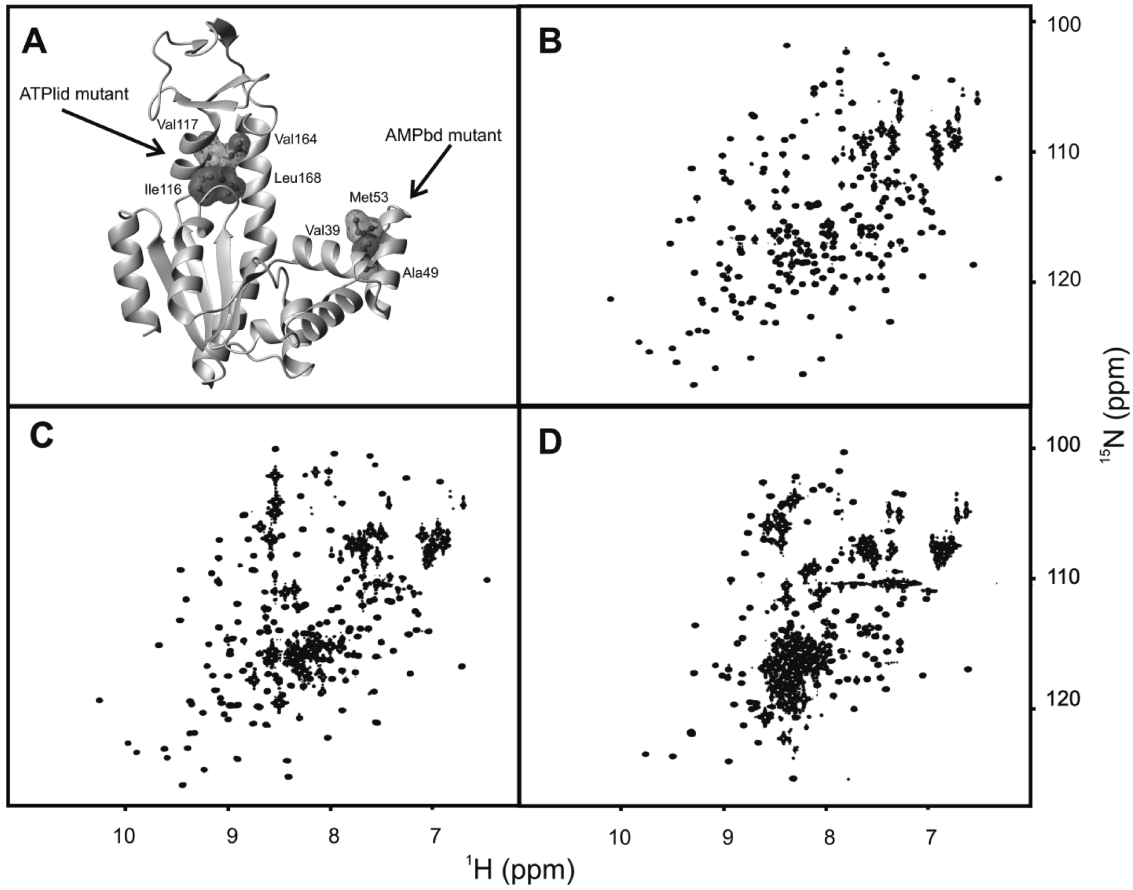

FIGURE 8: Structural location and NMR spectra of the ATPlid and AMPbd mutants. (A) Locations of the ATPlid and AMPbd mutants shown on the open mesoAdk structure with gray surface envelopes representing hydrophobic clusters that are perturbed. In the ATPlid mutant, Ile116, Val117, Val164, and Leu168 are replaced with glycine, and in the AMPbd mutant, Val39, Ala49, and Met53 are replaced with glycine. (B) ^{1}H−^{15}N HSQC spectrum of wild-type mesoAdk. (C) ^{1}H−^{15}N HSQC spectrum of the AMPbd mutant. (D) ^{1}H−^{15}N HSQC spectrum of the ATPlid mutant.

of the individual subdomains occurs in a noncooperative manner. If this hypothesis is correct, it should be possible to selectively unfold the flexible ATPlid and AMPbd subdomains without affecting the structural integrity of the CORE subdomain. Inspection of the crystallographic substrate-free mesoAdk structure reveals the presence of two hydrophobic clusters, one in ATPlid and another in AMPbd (Figure 8A). These clusters were selectively perturbed in two distinct mesoAdk mutants by replacing nonpolar amino acid residues with glycine. Glycine was chosen because this particular amino acid is known to have a large destabilizing effect on α-helices (*34*). Residues Val39, Ala49, and Met53 (AMPbd mutant) and Ile116, Val117, Val164, and Leu168 (ATPlid mutant) were mutated into glycine. The ^{1}H−^{15}N HSQC spectrum of the AMPbd mutant is similar to the wild-type spectrum, with the exception of several intense peaks positioned in the random coil region of the spectrum (Figure 8B,C). High peak intensities indicate that a specific amino acid residue displays increased motional degrees of freedom on the picosecond to nanosecond time scale, a feature expected for unfolded residues. Judging by the ^{1}H−^{15}N HSQC spectrum, it appears that the major fraction of residues in the AMPbd mutant is populating the native fold whereas some residues are populating an unfolded conformation. For the ATPlid mutant, a greater number of intense peaks in the ^{1}H−^{15}N HSQC is observed (Figure 8D), indicating that a larger part of the protein is unfolded compared to the AMPbd mutant. The presence of peaks with chemical shifts close to those of wild-type mesoAdk suggests that the mutant proteins in part retain correct native topology. To identify unfolded and correctly folded residues in the mutated proteins, ^{15}N T_2 relaxation lifetimes and C^{α} chemical shifts were compared between mutant and wild-type Adk. ^{15}N T_2 relaxation lifetimes are sensitive to motion on the picosecond to nanosecond time scale, and unfolded residues should display increased motion on this time scale compared to correctly folded residues, resulting in significantly increased relaxation lifetimes (*27*). C^{α} chemical shifts are highly sensitive to backbone torsion angles and can be used to predict secondary structure by using the chemical shift index (CSI) approach (*38*). To directly compare the topology of the wild type and mutated variants, the C^{α}-based CSI was generated. As a control of this method in Adk, the secondary structure of wild-type mesoAdk was predicted (Figure 9A,B). All secondary structure elements with the exception of β_F and β_G in the ATPlid matched the crystallographically determined secondary structure. A second anomaly is that residues 99−103 were identified as a β-strand, which can be explained by the extended conformation of this loop segment. The predicted secondary structure of the AMPbd mutant is very similar to the wild-type prediction with exception of residues 38−42 (α_2) and 44−54 (α_3) that are identified as a coil in the AMPbd, instead of the helical conformation identified in the wild type (Figure 9C,D). This result indicates that part of α_2 and the entire α_3 are unfolded in the AMPbd mutant. In the ATPlid mutant no secondary structure could be

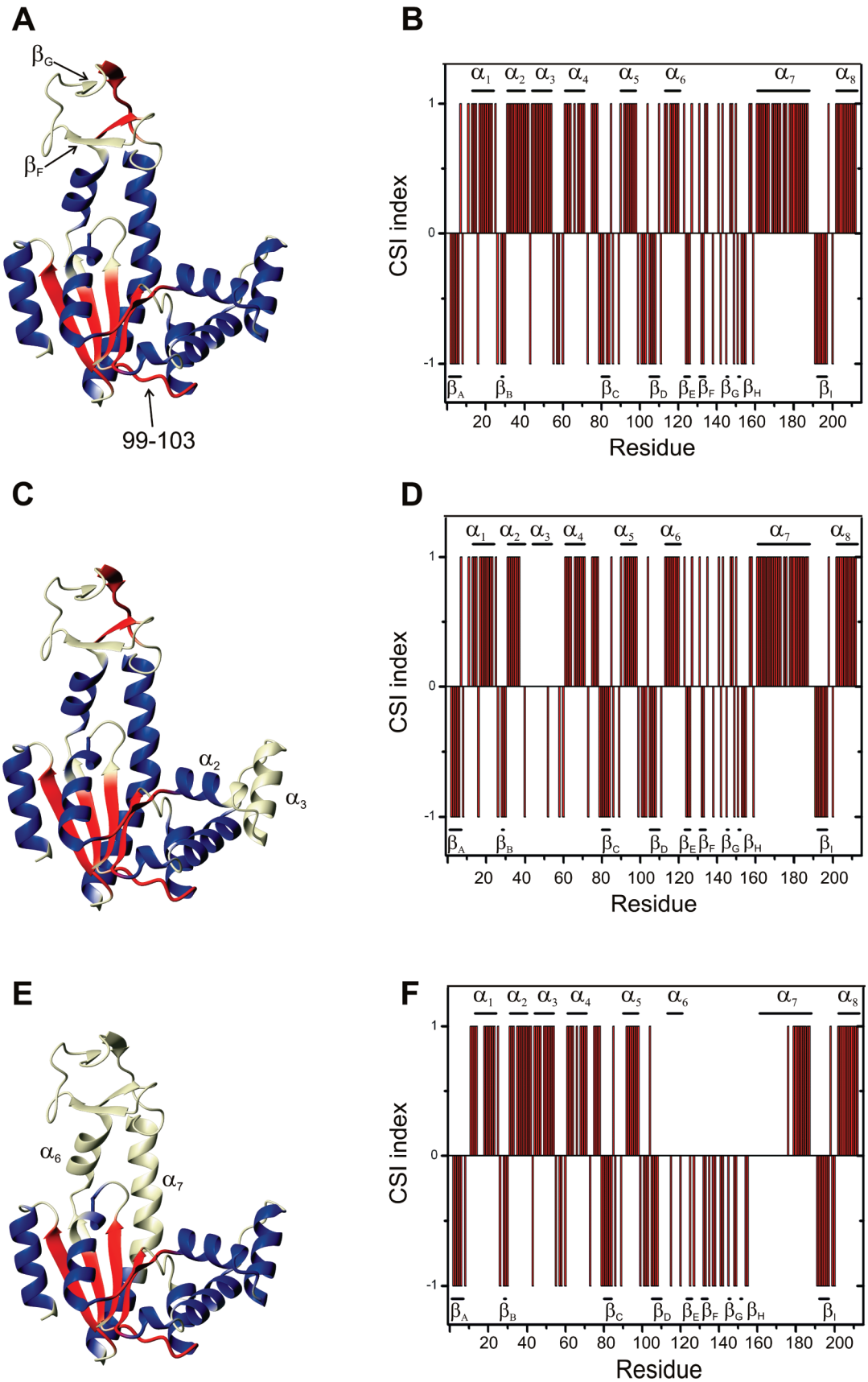

FIGURE 9: Analysis of C^{α} chemical shifts in wild-type and mutant mesoAdk. (A, C, E) Secondary structure predicted by CSI using C^{α} chemical shifts for wild type, AMPbd mutant, and ATPlid mutant, respectively. Residues that were predicted as α-helix (blue), β-strand (red), or coil (white) are shown on the crystallographic mesoAdk structure. Secondary structure elements were identified using MolMol. The loop region 99−103 and strands β_F and β_G are indicated in (A), α_2 and α_3 are indicated in (C), and α_6 and α_7 are indicated in (E). (B, D, F) C^{α} chemical shift based CSI index plot of wild type, AMPbd mutant, and ATPlid mutant, respectively. All regular secondary structure elements are indicated in the plot.

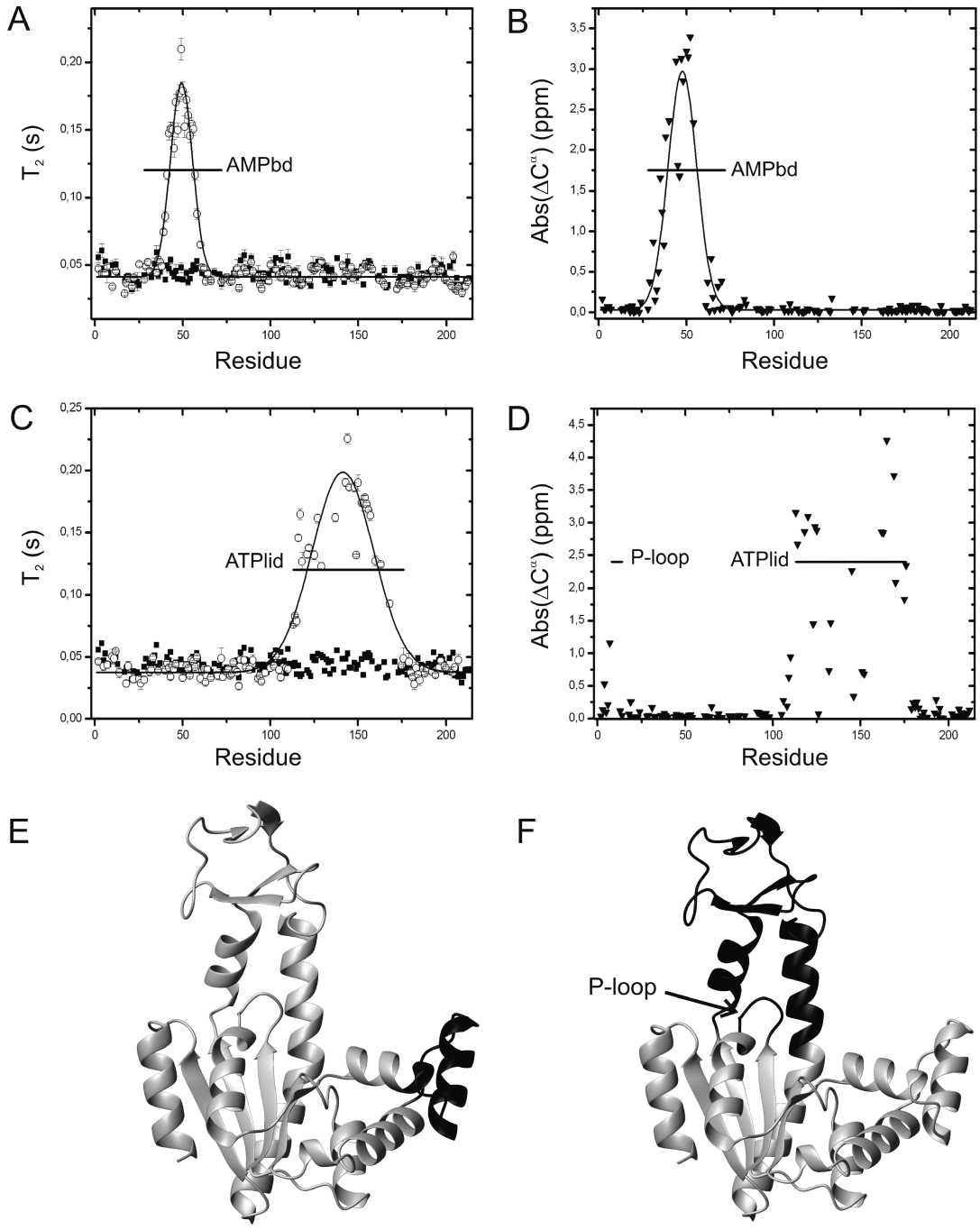

FIGURE 10: Identification of unfolded residues in the ATPlid and AMPbd mutants. (A) T_2 relaxation lifetimes of the AMPbd mutant (○) and wild-type mesoAdk (■). (B) Absolute values of C^α chemical shift differences between the AMPbd mutant and wild-type mesoAdk. (C) T_2 relaxation lifetimes of the ATPlid mutant (○) and wild-type mesoAdk (■). (D) Absolute values of C^α chemical shift differences between the ATPlid mutant and wild-type mesoAdk. C^α chemical shift differences are only shown for nonmutated residues in secondary structure elements identified in the substrate-free mesoAdk structure. (E) Structural location of residues 38−60 that are unfolded in the AMPbd mutant (black). (F) Structural location of residues 111−172 that are unfolded in the ATPlid mutant (black). In (A), (B), and (C), the fitted Gaussian distributions are indicated as solid lines. AMPbd is indicated in (A) and (B), ATPlid is indicated in (C) and (D), and the P-loop is indicated in (D) and (F).

identified for residues 113−178, whereas all other predicted secondary structure elements are virtually identical to the wild type (Figure 9E,F). Taken together, the CSI analysis indicates that the entire ATPlid (defined as residues 113−176) is unfolded in the ATPlid mutant.

In Figure 10A, ^{15}N T_2 relaxation lifetimes are shown for both wild-type mesoAdk and the AMPbd mutant. For wild-type Adk, the relaxation lifetimes are fluctuating around an average value of 44 ± 6 ms, indicating that the relaxation is dominated by global tumbling of the molecule and that all residues in wild-type mesoAdk are folded. It has been shown previously with relaxation dispersion experiments that the ^{15}N T_2 spin relaxation rate contains contributions from the conformational exchange process between open and closed mesoAdk that occurs in the substrate-free state (*5*). The relaxation experiment performed in this study is however performed with a Carr−Purcell−Meiboom−Gill field strength that effectively refocuses the contribution from conformational averaging, thus eliminating the contribution to T_2 relaxation rates from opening and closure of the ATPlid and

AMPbd. Residues in CORE and ATPlid in the AMPbd mutant display T_2 lifetimes that are strikingly similar to those of the wild type, suggesting that these subdomains have the correct native fold in the AMPbd mutant. In sharp contrast, many residues in the AMPbd subdomain have significantly longer T_2 lifetimes, which are indicative of unfolded residues. The residue-specific T_2 lifetimes gradually increase as a function of the distance to the structured part of the protein, which can be expected from a random coil that is constrained at the ends. The residue-specific relaxation lifetimes of the AMPbd mutant were fitted to a Gaussian distribution centered on residue Gly49, with a standard deviation of 13 residues. Residues are considered to be unfolded if the T_2 relaxation lifetimes obtained from the Gaussian fit are larger than five standard deviations (30 ms) above the mean T_2 lifetime (42 ms) for folded residues in the AMPbd mutant. Using this approach, we conclude that residues 38−60 are unfolded in the AMPbd mutant, in good agreement with the CSI analysis that showed loss of helical structure for residues 38−42 and 44−54. The discrepancy, i.e., residues 55−60, is due to the fact that these residues are predicted as a coil also in the wild-type protein using the CSI. Compared to the definition of AMPbd (residues 31−72), our results show that a section of the AMPbd subdomain is unfolded in the AMPbd mutant (Figure 10E). In Figure 10B, the absolute difference between C^α chemical shifts in wild-type mesoAdk and the AMPbd mutant for nonmutated residues that are populating secondary structure elements in the substrate-free X-ray structure is plotted as a function of the primary sequence position. Overall, the differences in chemical shift are small at all positions except for residues in the AMPbd subdomain. The conservation of C^α shifts outside of AMPbd shows that CORE and ATPlid do indeed retain the native fold in the AMPbd mutant. For residues in AMPbd, the chemical shift differences show a distribution that resembles the distribution of T_2 relaxation lifetimes and can be fitted to a Gaussian distribution centered on residue Lys47 with a standard deviation of 16 residues. The parameters in the Gaussian fit to both T_2 relaxation lifetimes and C^α chemical shift differences are strikingly similar, suggesting that the identification of unfolded residues based on T_2 relaxation lifetimes is an appropriate procedure.

In the ATPlid mutant, identification of folded and unfolded residues was accomplished by analyzing ^{15}N T_2 relaxation lifetimes. The relaxation lifetimes show good agreement between wild-type mesoAdk and the ATPlid mutant for residues in CORE and AMPbd subdomains, suggesting that these residues retain the native fold in the mutant protein (Figure 10C). Residues that are located within ATPlid show significantly increased relaxation lifetimes compared to wild-type mesoAdk, and the general pattern with a bell-like distribution of lifetimes similar to that of the AMPbd mutant is also observed for the ATPlid mutant. The residue-specific distribution of T_2 values in the ATPlid mutant was fitted to a Gaussian distribution centered on residue Lys141, with a standard deviation of 35 residues. Using the same argument as above, the relaxation data suggest that residues 111−172 are unfolded in the ATPlid mutant (Figure 10F), where ATPlid is defined as residues 113−176. Taken together with the CSI prediction, it is evident that the ATPlid is unfolded in the ATPlid mutant. Clearly, the number of unfolded residues in the ATPlid mutant is greater than in the AMPbd mutant. Analysis of C^α chemical shifts (performed as for the AMPbd mutant) for residues in AMPbd and CORE shows that residues in these regions have the correct native Adk fold in the ATPlid mutant. The only residues outside of ATPlid that show significant C^α chemical shift differences are residues Ile4 and Gly7, which are located immediately before the P-loop, and the origin of these perturbations is probably the close proximity to ATPlid, which is unfolded in the mutant protein (Figure 10F). Residues in ATPlid show a more complex distribution of C^α chemical shift differences compared to the relaxation lifetimes (Figure 10D) and could not be fitted to a Gaussian distribution.

The results from both protein engineering experiments show that folding of the CORE subdomain into the correct structure does not depend on the ATPlid or the AMPbd subdomain; evidently, there is no requirement for preformed structure in either of these flexible subdomains for proper folding of the CORE subdomain. In addition, ATPlid and AMPbd fold independently of each other. Taken together, these experiments point toward a model where the individual subdomains of Adk fold in a noncooperative manner.

DISCUSSION

Conformational change is crucial for the biological activity of a large number of proteins and enzymes. Relatively little is known about how polypeptide segments that participate in conformational changes are structurally consolidated in relation to the global protein folding trajectory. To address this question, we have taken an initial step by analyzing the folding cooperativity of individual subdomains in the enzyme Adk, a system where large-scale conformational changes are intimately linked to enzymatic activity. Experimentally, this question was approached by performing an NMR and protein engineering based folding study of Adk isolated from both mesophilic and hyperthermophilic bacteria. Overall, the hyperthermophilic enzyme displays an increased themodynamic stability for all subdomains which is expected given that the habitat temperatures are 95 (*39*) and 37 °C for *A. aeolicus* and *E. coli*, respectively. However, the structural distribution of local stabilities is strikingly similar between mesoAdk and thermoAdk with CORE being the most stable subdomain and the nucleotide binding domains displaying significantly reduced stabilities. Parts of the enzyme which display low thermodynamic stability in our experiments also show a striking similarity to the magnitude of the backbone nitrogen *B*-factors in the crystallographic mesoAdk substrate-free structure (*7*) (compare Figures 11 and 5A). The highest *B*-factors are observed in the flexible nucleotide binding subdomains; thus there exists an interesting correlation between dynamics in solution and in the crystal lattice. It has previously been shown that thermophilic ribonuclease H is stabilized in a delocalized fashion throughout the structure compared to a mesophilic variant (*40*). The results for Adk and ribonuclease H indicate that this may be a general way for thermophilic and hyperthermophilic enzymes to obtain their remarkable thermodynamic and thermal stabilities. Given the converging results in terms of structural distribution of local stabilities in mesoAdk and thermoAdk, the discussion below concerning folding cooperativity of subdomains is based on data obtained from both enzymes. It is important to note that our data provide a measure of

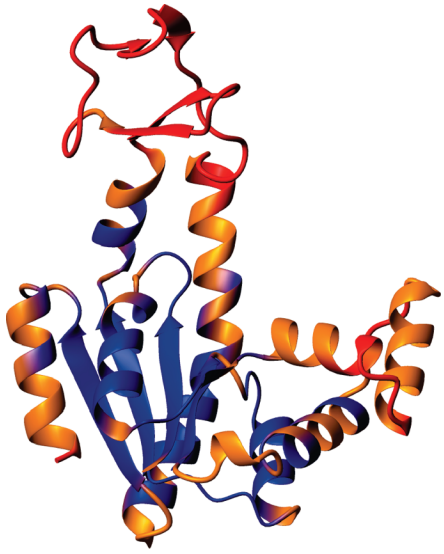

FIGURE 11: *B*-factor distribution of the open mesoAdk structure. Backbone nitrogen *B*-factors are displayed on 4AKE.pdb and are color-coded as follows: red, $B > 50$; orange, $50 > B > 30$; blue, $B < 30$.

the free energy differences between folded and unfolded ensembles of the individual subdomains but do not provide information about folding kinetics.

CORE was found to be the most stable subdomain in the Adk variants investigated. The high spatial resolution of the NMR folding experiments enabled a more detailed description of the CORE subdomain than is possible from inspection of crystallographic structures (Figure 1). Our experiments suggest that CORE is composed of two distinct foldons. m_{HX} values of residues in foldon 1 determined by equilibrium hydrogen exchange experiments are in good agreement with global values measured using CD spectroscopy, an indication that global unfolding of Adk mainly reports on the stability of CORE. Experiments performed using chimeric Adk variants show that the CORE subdomain determines the global melting temperature of the enzyme (*41*), an observation that is in good agreement with our results. Surprisingly, a few residues in AMPbd thermodynamically belong to foldon 1 of the CORE subdomain. The identification of a second foldon in the CORE subdomain suggests that the native structure of CORE is assembled with at least two distinct transitions. Haas and co-workers have studied the folding kinetics of the CORE subdomain in mesoAdk with time-resolved dynamic nonradiative excitation energy transfer experiments (*42*). These experiments have shown that CORE folds with at least two distinct transitions. During the first phase that occurred within the dead time of the experimental setup (less than 10 ms), the CORE subdomain collapsed into a compact structure with a short end to end distance. Helix α_7, which connects ATPlid with CORE and strand β_1 (Figure 1), remained in an unfolded conformation during this fast phase. These secondary structure elements gain their native structures during the following slow phase that was estimated to be on the order of 0.3−0.5 s^{-1} (*42*). Notably, the C-terminal part of helix α_7 and the entire strand β_1 belong to foldon 2 identified in our study (Figure 7C); thus the two-step kinetic folding behavior qualitatively agrees with the finding of two separate foldons in the CORE subdomain.

Disruption of structural integrity of ATPlid and AMPbd using mutagenesis resulted in selective unfolding of these subdomains. In both mutant proteins, analysis of T_2 relaxation lifetimes and C^α chemical shifts clearly shows that the CORE subdomain folds independently of the flexible subdomains.

Thermodynamically, ATPlid is less stable than the CORE subdomain and could be identified as a separate foldon. This foldon is associated with a hydrophobic cluster comprising the residues that were perturbed in the ATPlid mutant (Figure 8A). ^{15}N T_2 relaxation lifetimes and CSI analysis in the ATPlid mutant suggest that residues 111−172 are selectively unfolded, buttressing the inference that ATPlid is a cooperatively folding unit. In addition, the protein engineering experiments show that selective unfolding of AMPbd does not influence the structural integrity of ATPlid; thus the ATPlid subdomain folds independently of AMPbd.

AMPbd also has an overall thermodynamic stability that is lower than that of the CORE subdomain, and as mentioned above, part of helix α_4 thermodynamically belongs to foldon 1. Due to the fast hydrogen exchange rates of most residues in the AMPbd subdomain in mesoAdk, we were unable to identify AMPbd as a foldon by analyzing the denaturant dependency of ΔG_{HX}. Although AMPbd could not be identified as a foldon thermodynamically, a part of this subdomain could be selectively unfolded by destabilizing mutations. ^{15}N T_2 relaxation lifetimes and C^α chemical shifts in the AMPbd mutant show that residues 38−60 are unfolded in this mutated Adk variant. Furthermore, the AMPbd subdomain retains the native fold when ATPlid is selectively unfolded, showing that AMPbd folds independently of ATPlid. The overall reduced thermodynamic stabilities of ATPlid and AMPbd and the identification of ATPlid as a foldon, together with the fact that these subdomains in part can be selectively unfolded, suggest that the individual subdomains of Adk fold in a noncooperative manner. For an idealized two-state folding model, unfolding of one subdomain would provoke unfolding of the entire molecule. There exists evidence for noncooperative folding in other enzymes as well; for example, rabbit muscle aldolase has been shown to contain three domains within the same polypeptide chain that unfold sequentially. For aldolase the sequential unfolding was probed using amide hydrogen/mass spectrometry (*43, 44*). It is noteworthy that the noncooperatively folding subdomains in Adk are part of the same polypeptide chain and that the conformational dynamics of the nucleotide binding domains are linked to the catalytic activity of the enzyme. Hence for Adk it is possible to correlate the cooperativity of the folding reaction with the large-scale conformational change that is associated with enzymatic activity.

The crystallographic structures of open and closed Adk provide detailed structural descriptions of the extremes on the reaction pathway for closure of the substrate binding subdomains (Figure 1). Closure is associated with changes in local backbone conformation at several hinge regions (*45*); these hinge regions are shown on the open mesoAdk structure in Figure 12A. Even though the hinge regions have been identified with high precision, there exists no direct experimental evidence on the molecular details of the conformational change upon closure of Adk. Based on comparisons between ligand free and various ligand bound states, the segment movement between hinges in the NMP kinase family has been suggested to be rigid body translations following changes in local backbone conformation at the

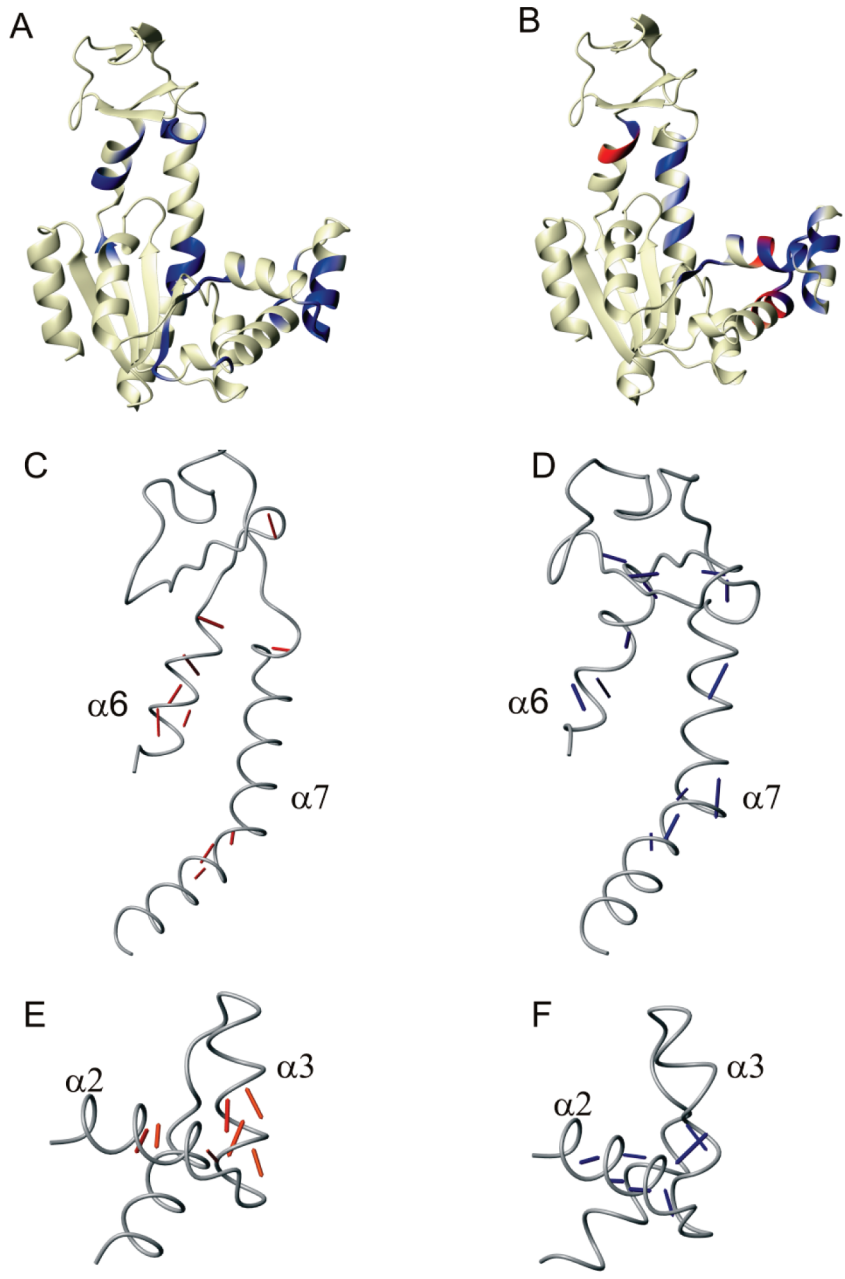

FIGURE 12: Hinge regions, local unfolding (cracking), and change in backbone hydrogen patterns for the open to closed transition of ATPlid and AMPbd in mesoAdk. (A) Hinge regions colored blue are adapted from ref *45*. (B) Residues suggested to undergo localized unfolding upon closure of ATPlid and AMPbd: (red) $\langle D_{max} \rangle$ larger than 0.2 radians; (blue) $\langle D_{max} \rangle$ between 0.05 and 0.2 radians as calculated by Whitford et al. (*47*). The average value of $\langle D_{max} \rangle$ for the open−open ensemble was subtracted out from the data reported in Whitford et al., Figure 5 (personal communication). (C, D) Illustration of backbone hydrogen bonds that is present only in either open or closed Ap5A-bound mesoAdk. In the analysis both chains A and B in 1AKE are considered. Hydrogen bonds were identified with MolMol. (C) Hydrogen bonds present only in the ATPlid of open mesoAdk. (D) Hydrogen bonds present only in the ATPlid of closed mesoAdk. (E) Hydrogen bonds present only in the AMPbd of open mesoAdk. (F) Hydrogen bonds present only in the AMPbd of closed mesoAdk.

hinge regions (*9, 46*), in essence an induced fit model. There also exists an alternative view on the mechanism of conformational change; recent theoretical approaches suggest that many residues in both ATPlid and AMPbd experience high strain energy on the reaction trajectory from the open to the closed conformation. The unfavorable strain is suggested to be relieved by local unfolding of a number of residues (Figure 12B), suggesting that the conformational change in Adk in part is a folding/unfolding reaction (*47*−*49*). These functional local unfolding events have been named "cracking" to differentiate from global unfolding of the entire molecule (*47*). Cracking is qualitatively buttressed with the observation that Adk becomes 1.6-fold more active in the presence of 1 M urea (*50*). Addition of denaturant can in principle act to lower the free energy barrier of the localized folding/unfolding reaction. Comparison of ATPlid and AMPbd in open and closed mesoAdk reveals that there are significant changes in the backbone hydrogen-bonding pattern between these states (Figure 12C−F). Thus hydrogen bonds are being broken and re-formed on the reaction trajectory, and these rearrangements in hydrogen bonds contribute to the activation energy barriers that must be overcome for opening and closing of the enzyme. In ATPlid the shift in hydrogen-bonding pattern is localized primarily to α_6 and α_7 and in the AMPbd to α_2 and α_3. The rearrangement in hydrogen-bonding patterns in ATPlid and

AMPbd upon closure infers that hydrogen bonds must be allowed to break on a pathway that is distinct to the global unfolding trajectory in order to avoid complete unfolding of the entire molecule during the conformational changes.

Noncooperative folding together with reduced thermodynamic stability of the substrate binding subdomains has the functional advantage of allowing rearrangement of hydrogen-bonding patterns and cracking during conformational changes without provoking global unfolding of the entire molecule. It is also possible that the local fluctuations present in Adk under native conditions are functionally relevant and enable the change in hydrogen-bonding pattern (cracking) during conformational change. Protein folding is the result of a delicate balance between large stabilizing and destabilizing forces (*34*). Our results suggest that segments that undergo conformational change also depend on a fine-tuning of thermodynamic stability relative to the global stability. As a concluding remark, we speculate that noncooperative folding of mobile segments may be relevant not only for enzymes but also more generally for proteins that require conformational changes for biological activity.

ACKNOWLEDGMENT

José N. Onuchic and Paul C. Whitford are acknowledged for assistance with preparation of Figure 12B. We thank Elisabeth Sauer-Eriksson for valuable comments during the preparation of the manuscript. Yawen Bai is acknowledged for help with interpretation of hydrogen exchange experiments.

SUPPORTING INFORMATION AVAILABLE

Fitted thermodynamic parameters extracted from hydrogen to deuterium exchange experiments (Tables S1−S3). This material is available free of charge via the Internet at http://pubs.acs.org.

REFERENCES

1. Boehr, D. D., Dyson, H. J., and Wright, P. E. (2006) An NMR perspective on enzyme dynamics. *Chem. Rev. 106*, 3055–3079.
2. Eisenmesser, E. Z., Millet, O., Labeikovsky, W., Korzhnev, D. M., Wolf-Watz, M., Bosco, D. A., Skalicky, J. J., Kay, L. E., and Kern, D. (2005) Intrinsic dynamics of an enzyme underlies catalysis. *Nature 438*, 117–121.
3. Beach, H., Cole, R., Gill, M. L., and Loria, J. P. (2005) Conservation of μs-ms enzyme motions in the apo- and substrate-mimicked state. *J. Am. Chem. Soc. 127*, 9167–9176.
4. Labeikovsky, W., Eisenmesser, E. Z., Bosco, D. A., and Kern, D. (2007) Structure and dynamics of pin1 during catalysis by NMR. *J. Mol. Biol. 367*, 1370–1381.
5. Henzler-Wildman, K. A., Thai, V., Lei, M., Ott, M., Wolf-Watz, M., Fenn, T., Pozharski, E., Wilson, M. A., Petsko, G. A., Karplus, M., Hübner, C. G., and Kern, D. (2007) Intrinsic motions along an enzymatic reaction trajectory. *Nature 450*, 838–844.
6. Rhoads, D. G., and Lowenstein, J. M. (1968) Initial velocity and equilibrium kinetics of myokinase. *J. Biol. Chem. 243*, 3963–3972.
7. Müller, C. W., Schlauderer, G. J., Reinstein, J., and Schulz, G. E. (1996) Adenylate kinase motions during catalysis: an energetic counterweight balancing substrate binding. *Structure 4*, 147–156.
8. Müller, C. W., and Schulz, G. E. (1992) Structure of the complex between adenylate kinase from *Escherichia coli* and the inhibitor Ap5A refined at 1.9 Å resolution. A model for a catalytic transition state. *J. Mol. Biol. 224*, 159–177.
9. Vonrhein, C., Schlauderer, G. J., and Schulz, G. E. (1995) Movie of the structural changes during a catalytic cycle of nucleoside monophosphate kinases. *Structure 3*, 483–490.
10. Wolf-Watz, M., Thai, V., Henzler-Wildman, K., Hadjipavlou, G., Eisenmesser, E. Z., and Kern, D. (2004) Linkage between dynamics and catalysis in a thermophilic-mesophilic enzyme pair. *Nat. Struct. Mol. Biol. 11*, 945–949.
11. Ådén, J., and Wolf-Watz, M. (2007) NMR identification of transient complexes critical to adenylate kinase catalysis. *J. Am. Chem. Soc. 129*, 14003–14012.
12. Whitford, P. C., Gosavi, S., and Onuchic, J. N. (2008) Conformational transitions in adenylate kinase: allosteric communication reduces misligation. *J. Biol. Chem. 283*, 2042–2048.
13. Vuister, G. W., and Bax, A. (1993) Quantitative J correlation: a new approach for measuring homonuclear 3-bond J(H(N)H(alpha) coupling-constants in N-15-enriched proteins. *J. Am. Chem. Soc. 115*, 7772–7777.
14. Farrow, N. A., Muhandiram, R., Singer, A. U., Pascal, S. M., Kay, C. M., Gish, G., Shoelson, S. E., Pawson, T., Forman-Kay, J. D., and Kay, L. E. (1994) Backbone dynamics of a free and a phosphopeptide-complexed Src homology-2 domain studied by N-15 NMR relaxation. *Biochemistry 33*, 5984–6003.
15. Delaglio, F., Grzesiek, S., Vuister, G. W., Zhu, G., Pfeifer, J., and Bax, A. (1995) NMRPipe: a multidimensional spectral processing system based on UNIX pipes. *J. Biomol. NMR 6*, 277–293.
16. Helgstrand, M., Kraulis, P., Allard, P., and Härd, T. (2000) Ansig for Windows: an interactive computer program for semiautomatic assignment of protein NMR spectra. *J. Biomol. NMR 18*, 329–336.
17. Grzesiek, S., and Bax, A. (1992) Improved 3D triple-resonance NMR techniques applied to a 31-Kda protein. *J. Magn. Reson. 96*, 432–440.
18. Wittekind, M., and Mueller, L. (1993) HNCACB, a high-sensitivity 3D NMR experiment to correlate amide-proton and nitrogen resonances with the alpha-carbon and beta-carbon resonances in proteins. *J. Magn. Res., Ser. B 101*, 201–205.
19. Grzesiek, S., and Bax, A. (1992) Correlating backbone amide and side-chain resonances in larger proteins by multiple relayed triple resonance NMR. *J. Am. Chem. Soc. 114*, 6291–6293.
20. Farmer, B. T., and Venters, R. A. (1995) Assignment of side-chain C-13 resonances in perdeuterated proteins. *J. Am. Chem. Soc. 117*, 4187–4188.
21. Schanda, P., and Brutscher, B. (2005) Very fast two-dimensional NMR spectroscopy for real-time investigation of dynamic events in proteins on the time scale of seconds. *J. Am. Chem. Soc. 127*, 8014–8015.
22. Connelly, G. P., Bai, Y. W., Jeng, M. F., and Englander, S. W. (1993) Isotope effects in peptide group hydrogen-exchange. *Proteins: Struct., Funct., Genet. 17*, 87–92.
23. Bai, Y., Sosnick, T. R., Mayne, L., and Englander, S. W. (1995) Protein folding intermediates: native-state hydrogen exchange. *Science 269*, 192–197.
24. Chamberlain, A. K., Handel, T. M., and Marqusee, S. (1996) Detection of rare partially folded molecules in equilibrium with the native conformation of RNaseH. *Nat. Struct. Biol. 3*, 782–787.
25. Press, W. H., Teukolsky, S. A., Vetterling, W. T., and Flannery, B. P. (1992) *Numerical recipes in C. The art of scientific computing*, 2nd ed., Cambridge University Press, Cambridge, U.K.
26. Englander, S. W., and Kallenbach, N. R. (1984) Hydrogen exchange and structural dynamics of proteins and nucleic acids. *Q. Rev. Biophys. 16*, 521–655.
27. Takei, J., Pei, W., Vu, D., and Bai, Y. (2002) Populating partially unfolded forms by hydrogen exchange-directed protein engineering. *Biochemistry 41*, 12308–12312.
28. Bédard, S., Mayne, L. C., Peterson, R. W., Wand, A. J., and Englander, S. W. (2008) The foldon substructure of staphylococcal nuclease. *J. Mol. Biol. 376*, 1142–1154.
29. Bai, Y., Milne, J. S., Mayne, L., and Englander, S. W. (1994) Protein stability parameters measured by hydrogen exchange. *Proteins: Struct., Funct., Genet 20*, 4–14.
30. Hvidt, A., and Nielsen, S. O. (1966) Hydrogen exchange in proteins. *Adv. Protein Chem. 21*, 287–386.
31. Bai, Y., Milne, J. S., Mayne, L., and Englander, S. W. (1993) Primary structure effects on peptide group hydrogen exchange. *Proteins: Struct., Funct., Genet. 17*, 75–86.
32. Polshakov, V. I., Birdsall, B., and Feeney, J. (2006) Effects of co-operative ligand binding on protein amide NH hydrogen exchange. *J. Mol. Biol. 356*, 886–903.
33. Lienhard, G. E., and Secemski, I. I. (1973) P 1 P 5 -Di(adenosine-5′)pentaphosphate, a potent multisubstrate inhibitor of adenylate kinase. *J. Biol. Chem. 248*, 1121–1123.
34. Fersht, A. (2000) *Structure and mechanism in protein science*, W. H. Freeman, New York.

35. Maity, H., Lim, W. K., Rumbley, J. N., and Englander, S. W. (2003) Protein hydrogen exchange mechanism: Local fluctuations. *Protein Sci. 12*, 153–160.
36. Huyghues-Despointes, B. M., Scholtz, J. M., and Pace, C. N. (1999) Protein conformational stabilities can be determined from hydrogen exchange rates. *Nat. Struct. Biol. 6*, 910–912.
37. Reimer, U., Scherer, G., Drewello, M., Kruber, S., Schutkowski, M., and Fischer, G. (1998) Side-chain effects on peptidyl-prolyl cis/trans isomerisation. *J. Mol. Biol. 279*, 449–460.
38. Wishart, D. S., and Sykes, B. D. (1994) The ^{13}C chemical-shift index: a simple method for the identification of protein secondary structure using ^{13}C chemical-shift data. *J. Biomol. NMR 4*, 171–180.
39. Deckert, G., Warren, P. V., Gaasterland, T., Young, W. G., Lenox, A. L., Graham, D. E., Overbeek, R., Snead, M. A., Keller, M., Aujay, M., Huber, R., Feldman, R. A., Short, J. M., Olsen, G. J., and Swanson, R. V. (1998) The complete genome of the hyperthermophilic bacterium *Aquifex aeolicus*. *Nature 392*, 353–358.
40. Hollien, J., and Marqusee, S. (1999) Structural distribution of stability in a thermophilic enzyme. *Proc. Natl. Acad. Sci. U.S.A. 96*, 13674–13678.
41. Bae, E., and Phillips, G. N., Jr. (2006) Roles of static and dynamic domains in stability and catalysis of adenylate kinase. *Proc. Natl. Acad. Sci. U.S.A. 103*, 2132–2137.
42. Ratner, V., Amir, D., Kahana, E., and Haas, E. (2005) Fast collapse but slow formation of secondary structure elements in the refolding transition of *E. coli* adenylate kinase. *J. Mol. Biol. 352*, 683–699.
43. Deng, Y., and Smith, D. L. (1998) Identification of unfolding domains in large proteins by their unfolding rates. *Biochemistry 37*, 6256–6262.
44. Deng, Y., and Smith, D. L. (1999) Hydrogen exchange demonstrates three domains in aldolase unfold sequentially. *J. Mol. Biol. 294*, 247–258.
45. Henzler-Wildman, K. A., Lei, M., Thai, V., Kerns, S. J., Karplus, M., and Kern, D. (2007) A hierarchy of timescales in protein dynamics is linked to enzyme catalysis. *Nature 450*, 913–916.
46. Gerstein, M., Schulz, G., and Chothia, C. (1993) Domain closure in adenylate kinase. Joints on either side of two helices close like neighboring fingers. *J. Mol. Biol. 229*, 494–501.
47. Whitford, P. C., Miyashita, O., Levy, Y., and Onuchic, J. N. (2007) Conformational transitions of adenylate kinase: switching by cracking. *J. Mol. Biol. 366*, 1661–1671.
48. Miyashita, O., Onuchic, J. N., and Wolynes, P. G. (2003) Nonlinear elasticity, proteinquakes, and the energy landscapes of functional transitions in proteins. *Proc. Natl. Acad. Sci. U.S.A. 100*, 12570–12575.
49. Whitford, P. C., Onuchic, J. N., and Wolynes, P. G. (2008) Energy landscape along an enzymatic reaction trajectory: hinges or cracks? *HFSP J. 2*, 61–64.
50. Zhang, H. J., Sheng, X. R., Pan, X. M., and Zhou, J. M. (1997) Activation of adenylate kinase by denaturants is due to the increasing conformational flexibility at its active sites. *Biochem. Biophys. Res. Commun. 238*, 382–386.
51. Koradi, R., Billeter, M., and Wüthrich, K. (1996) MOLMOL: a program for display and analysis of macromolecular structures. *J. Mol.Graphics 14*, 29–32.
52. Santoro, M. M., and Bolen, D. W. (1988) Unfolding free-energy changes determined by the linear extrapolation method. 1. Unfolding of phenylmethanesulfonyl Alpha-chymotrypsin using different denaturants. *Biochemistry 27*, 8063–8068.

BI8018042